Fabrication and characterization of freestanding ultrathin diamond-like carbon targets for high-intensity laser applications

**Timothy T. Ho · Manisha Gupta ·
Fatema Rezwana Chowdhury ·
Zhijiang Chen · Ying Yin Tsui**

Abstract Here, we report the fabrication of diamond-like carbon (DLC) thin films using pulsed laser deposition (PLD). PLD is a well-established technique for deposition of high-quality DLC thin films. Carbon tape target was ablated using a KrF (248 nm, 25 ns, 20 Hz) excimer laser to deposit DLC films on soap-coated substrates. A laser fluence between 8.5 and 14 J/cm^2 and a target to substrate distance of 10 cm was used. These films were then released from substrates to obtain freestanding DLC thin foils. Foil thicknesses from 20 to 200 nm were deposited using this technique to obtain freestanding targets of up to 1-inch square area. Typically, 100-nm-thick freestanding DLC films were characterized using different techniques such as AFM, XPS, and nano-indentation. AFM was used to obtain the film surface roughness of 9 nm rms of the released film. XPS was utilized to obtain 74 % sp^2, 23 % sp^3, and 3 % C–O bond components. Nano-indentation was used to characterize the film hardness of 10 GPa and Young's modulus of 110 GPa. Damage threshold properties of the DLC foils were studied (1,064 nm, 6 ns) and found to be 7×10^{10} W/cm^2 peak intensity for our best ultrathin DLC foils.

Timothy T. Ho and Manisha Gupta equally contributed to this work.

T. T. Ho (✉) · M. Gupta · F. R. Chowdhury · Z. Chen · Y. Y. Tsui
Electrical and Computer Engineering, University of Alberta, Edmonton, AB T6G 2V4, Canada
e-mail: tho2@ualberta.ca

M. Gupta
e-mail: mgupta1@ualberta.ca

1 Introduction

Diamond-like carbon (DLC) films have been of interest for many years since they carry properties of both graphite and diamond forms of carbon. They have been used previously as stripper and stop foils in particle acceleration experiments [1]. Recently, there are great interests for using freestanding ultrathin DLC with thickness on the nanometer scale, as target for ultrahigh-intensity laser–matter interaction studies. It was discovered that the use of ultrathin targets allows new acceleration mechanisms, including the breakout afterburner (BOA) [2, 3] for linearly polarized laser beams and radiation pressure acceleration (RPA) [4] and soliton-driven ion acceleration [5, 6] for circularly polarized laser beams. It has been recently reported that fully ionized carbon ions and protons with maximum energy of 185 and 35 MeV, respectively, can be produced when ultrathin DLC foils are irradiated by high-contrast linearly polarized sub-picosecond ultrahigh-intensity laser pulses [3]. When circularly polarized laser beam was used, it resulted in lower maximum energy ions [6] but quasi-monoenergetic ions can be produced under proper conditions [7]. It was shown that quasi-monoenergetic carbon ions with an energy spread of as low as 15 % at 35 MeV could be produced [7]. Ultrashort multi-MeV pulsed protons have many important applications. Two of them are ion-driven fast ignition fusion and laser-driven ion therapy. The ion-driven fast ignition fusion [8] which looks to address an important issue has been attracting growing attention: the need for a clean, safe, and long-term energy source. Laser-driven ions for therapeutic applications have potential to reduce cost and physical footprint over typical cyclotron and synchrotron acceleration. Corresponding dosage from these pulsed ion beams was found not to differ in relative biological effectiveness compared to typical continuous sources [9]. Both of these

applications require high-quality freestanding ultrathin DLC films and these films must be robust enough to withstand the prepulse of the ultrahigh-intensity laser. The ultrahigh-intensity laser is typically preceded by a lower intensity prepulse, a few nanoseconds ahead of the main pulse [10]. Here, we present the fabrication, release, and characterization of freestanding ultrathin DLC foils grown using the pulsed laser deposition (PLD) technique. The characterization of the DLC film included several different techniques including atomic forcing microscopy (AFM), X-ray photoelectron spectroscopy (XPS), and nano-indentation. AFM was used to investigate surface roughness, XPS to obtain peak ratios of sp^2 and sp^3 peaks, and nano-indentation to characterize film strength. Of particular interest is investigating the damage threshold of the film. Since main pulse of the ultrahigh-intensity laser is led by a prepulse of notable intensity, a critical requirement of the film is for it to survive the prepulse. This property was studied using a 1,064 nm wavelength, nanosecond pulse, Q-switched Nd:YAG laser to simulate the prepulse.

2 Experimental techniques

2.1 PLD growth setup and conditions

The films presented here were grown using PLD. The substrate used was a soap-covered glass microscope slide. Then, a graphite carbon tape target was ablated by a KrF excimer laser (248 nm, 25 ns, 10 Hz) to deposit a DLC film onto the substrate. No hydrogen was added into the DLC film. The tape target was continuously scrolled during deposition to provide fresh surface for each laser pulse. During the deposition, a laser fluence of 8.5–14 J/cm^2 (0.34–0.56 GW/cm^2) was used with a target to substrate distance of 10 cm [11]. Once the film was grown, it was released from the substrate by dissolving the soap in warm distilled water, allowing the film to float on the water surface. The release technique is similar to one used in a different study [1]. Here, liquid soap was applied to a glass slide and polished until it was visually uniformly clouded over. The film was then lifted-off on to the metal plate (31.2 mm × 50.2 mm × 1.2 mm) with 7 × 15 square array of 500-μm-diameter holes spaced 3 mm apart. This allowed for freestanding films over the 500-μm-diameter holes to be available for testing. The lips of the holes were raised slightly to hold the film taut and reduce wrinkling.

2.2 Beam spot measurement of the Nd:YAG laser beam

The beam spot diameter of the Nd:YAG laser (Big Sky Laser Technologies) at 1,064 nm wavelength was measured
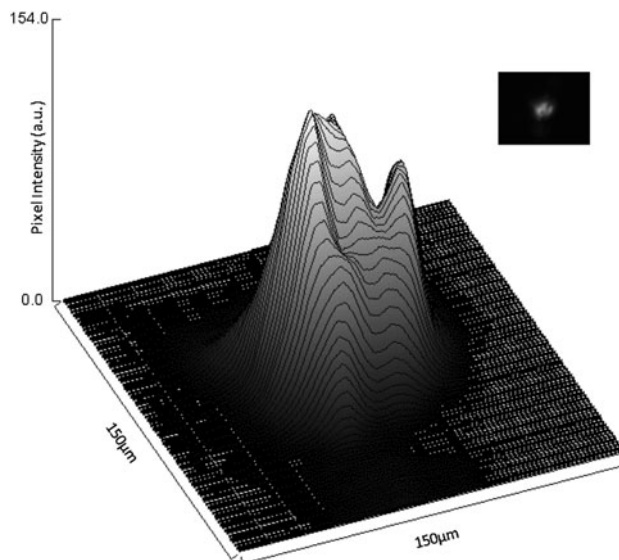

Fig. 1 Laser spot profile of 1,064 nm laser spot obtained using CCD camera to determine the laser fluence. The 90 % energy contour of the spot is roughly circular with 68 μm diameter

using a Chameleon monochromatic CCD from Point Grey Research. A 1-inch-diameter f/2, fused silica, plano-convex lens was used to focus the laser beam to the tightest spot and wedge windows were used with neutral density filters to prevent the CCD from saturating. This laser was used to simulate the prepulse.

The focused beam spot diameter was roughly circular in shape (∼68 μm diameter at 90 % energy contour) but contained features as can be seen in Fig. 1 which shows the representative laser spot profile measured using the CCD camera. Inset in Fig. 1 shows the image of the laser beam spot. The laser fluence was calculated using the energy contour area. The spatial profile of the laser is clearly multimodal, which would provide a reasonable model for simulating prepulses from ultrahigh-intensity lasers used for producing carbon ions. They are typically ∼1 μm wavelength range and normally do not have perfect Gaussian beam spots.

2.3 Setup for damage threshold measurement

The damage threshold characterization was carried out using a Q-switched Nd:YAG laser with 6 ns FWHM pulse width. Schematic of the experimental setup is shown in Fig. 2. Two 45° 1,064 nm mirrors were used to steer the laser beam and eliminate the 532 nm. Also, to further remove the remaining, 532 nm component long-pass filters of 590 and 610 nm were used. The laser beam was focused using a 1-inch-diameter f/2, fused silica, plano-convex lens. The sample holder was placed on an x–y–z translation stage at the best focus. A HeNe laser (632 nm) was used to assist
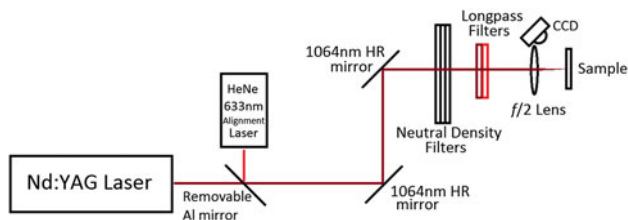
Fig. 2 Schematic of the setup to conduct the damage experiments, utilizing the 1,064 nm mirrors to steer the laser beam and then focus it on to the sample. Long-pass filters were used to filter the 532 nm component

with alignment, along with a CCD for viewing the laser spot location. Neutral density filters were used before the long-pass filters and varied to obtain the required fluence.

2.4 Film characterization

X-ray photoelectron spectroscopy was used to analyze the bonding proportion of the DLC film. The XPS measurements were taken on ULTRA spectrometer (Kratos Analytical) at the Alberta Center for Surface Science (ACSES), University of Alberta. Monochromatic Al Kα source (hν = 1,486.6 eV) was used at a power of 210 W. The analysis spot was 400 μm × 700 μm and take off angle was 90^0. The resolution of the instrument is 0.55 eV for Ag 3d and 0.7 eV for Au 4f peaks. The scan on DLC thin film was conducted with analyzer pass energy of 160 eV and high-resolution spectra with 20 eV. The data were collected after cleaning off the surface with Ar ion beam etching. CASA software was used for data processing and component analysis.

To determine the thin film hardness, nano-indentation was utilized. This was conducted using Hysitron TI900 TriboIndenter. A Berkovich tip was used to conduct the hardness experiments. The hardness of the thin films was measured by loading the sample from 100 to 4,500 μN force. Diamond should consist of a very high percentage of sp^3 bonds as compared to the sp^2 bonds in graphite. Thus, both of these techniques, XPS and nano-indentation, help in determining the thin film properties.

The AFM was conducted using DI 3,100 instrument. All the AFM scans were conducted using tapping mode. This was used to analyze the growth quality of the DLC film and the film quality after lift-off and to obtain surface roughness. Film thickness was measured using KLA Tencor Alpha Step IQ profilometer in different areas to determine the film uniformity.

Optical properties (n, k) were also investigated using a variable angle spectroscopic ellipsometer (VASE). Transmission of the DLC thin films grown on quartz substrate was conducted using an NIR-UV PerkinElmer Lambda 900 Spectrophotometer.

3 Results and discussion

3.1 Film characterization

Using AFM, the roughness of the DLC growth was obtained. Figure 3a shows the AFM images of the DLC film grown on Si substrate demonstrating a low rms roughness of 0.6 nm. The samples used for damage tests were grown on soap films on glass substrate, and the soap film demonstrated a roughness of 8–12 nm. Films were then lifted-off onto metal plates as described above. Figure 3b shows the image of the lifted-off film with a roughness of 9 nm, consistent with the soap film roughness. Since these are to be used as targets for lasers at wavelength of ∼1 μm, the roughness is about λ/100, which is acceptable. A range of DLC film thicknesses was grown and the step height of the film was measured using the Alpha Step IQ profilometer and found to be between 20 and 200 nm. Films with a thickness of 100 nm were typically used for characterization techniques.

X-ray photoelectron spectroscopy spectrum of the 100-nm-thick DLC film was measured as described in the experimental methods section. The sample was cleaned by sputtering with Ar ion beam and then the XPS spectrum was measured; this was done to ensure to remove the environmental carbon present on the surface. Figure 4 shows the XPS spectra of the DLC thin film showing sp^2 and sp^3 components. The Carbon 1s peak was then deconvoluted to determine the sp^2 (284.5 eV) and sp^3 (285.2 eV) components. The fractions of the sp^3 and sp^2 components were determined to be 23 and 74 %, respectively, along with the 3 % of C–O bonds. The fitting of the data has been conducted using a similar technique of three components as used in the study [11, 12]. This is consistent with our previous studies in which we found, at a slightly higher laser intensity of 0.7 GW/cm² and a smaller film thickness of 24 ± 5 nm, the sp^3 content was 40 ± 15 % by using electron energy loss spectroscopy (EELS) [13]. Since deposition occurred at a higher intensity, we expect the sp^3 bonding percentage to be higher as well.

Nano-indentation studies were conducted on both DLC thin films and on silicon nitride thin films both 100 nm thick. DLC films demonstrated an average hardness of 10 GPa for a force between 100 and 4,500 μN. The Young's modulus of the film was determined to be 110 GPa. From earlier studies, it was observed that the sp^3 content in the DLC films is extremely dependent on the laser fluence during the PLD process and the growth temperature. For laser fluence between 10 and 20 J/cm², a high sp^3 content of 85 % has been observed for a substrate temperature of 90 °C [14]. They also observe a hardness of 85 GPa and a Young's modulus of 900 GPa. We have a much lower sp^3 content and hence a lower hardness. This could be due to

AFM image of 2 μm × 2 μm area of the DLC film deposited on **a** Si substrate with an rms roughness of 0.6 nm **b** DLC film grown on soap film (rms roughness 8–12 nm) and lifted-off on to a metal plate demonstrating an rms roughness of 9 nm
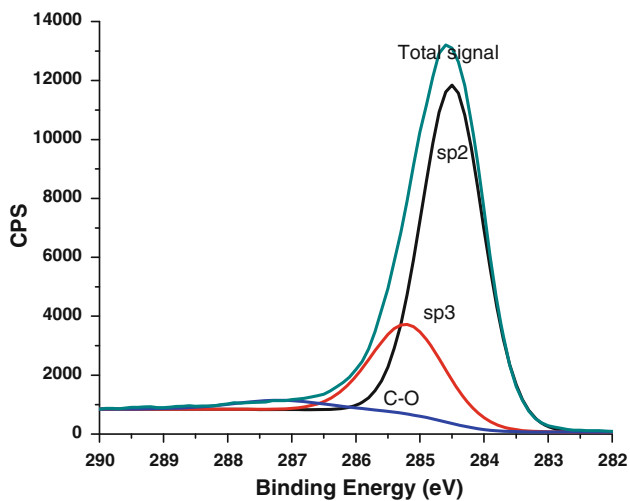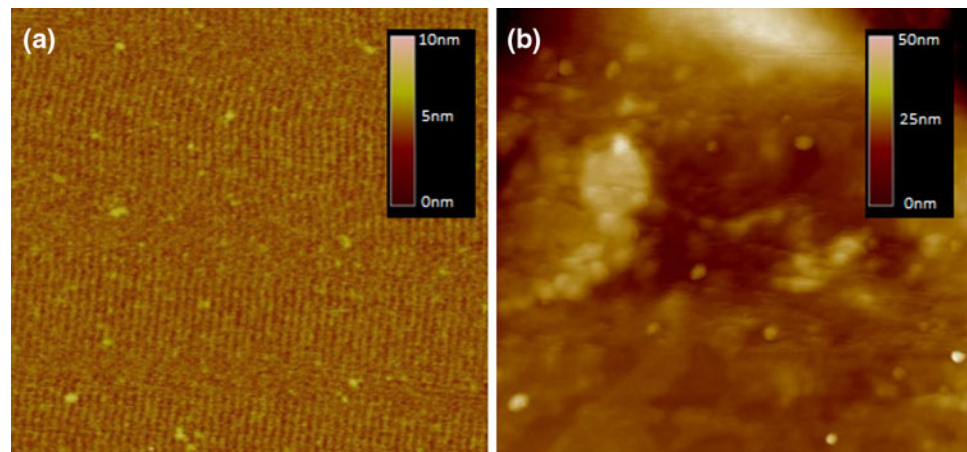

Fig. 4 XPS spectra of 100-nm-thick DLC film showing 23 % sp^3 and 74 % sp^2 and 3 % of C–O component

Fig. 5 VASE spectrum of 50 nm DLC film showing n, k for visible near-infrared region

the lower growth fluence and room temperature growths, which is similar to the hardness and Young's modulus observed in the study conducted on DLC films grown by ECR plasma CVD [15]. Additionally, the films are very thin and near the limit of the indentation procedure.

The VASE was used to determine the complex index of refraction in the visible near-infrared spectrum plotted in Fig. 5. In a wavelength range of 400–1,300 nm tested, the DLC film exhibited a range of 1.83–1.74 in index of refraction and 0.11–0 in extinction coefficient. As expected, the DLC film has poor absorption in the near-infrared region. Given the relatively lower sp^3 content of the film, lower index of refraction is expected. The values of n and k obtained here are similar to the ones obtained in earlier studies for lower sp^3 content [15, 16]. The spectrophotometer measured the transmission of 25 nm DLC grown on quartz substrate and is shown in Fig. 6. The film shows very high transparency compared with the quartz sample in the near-infrared region.
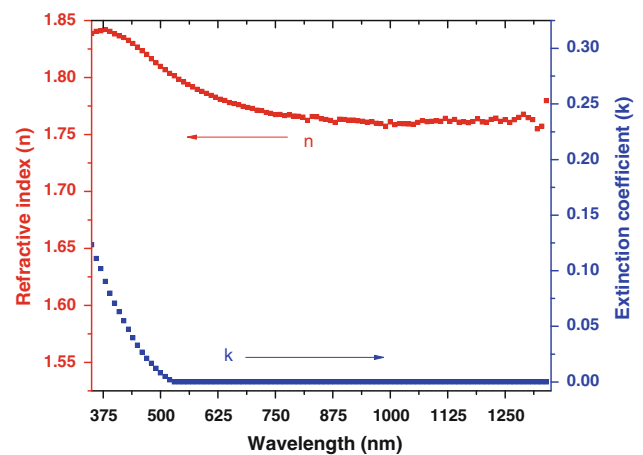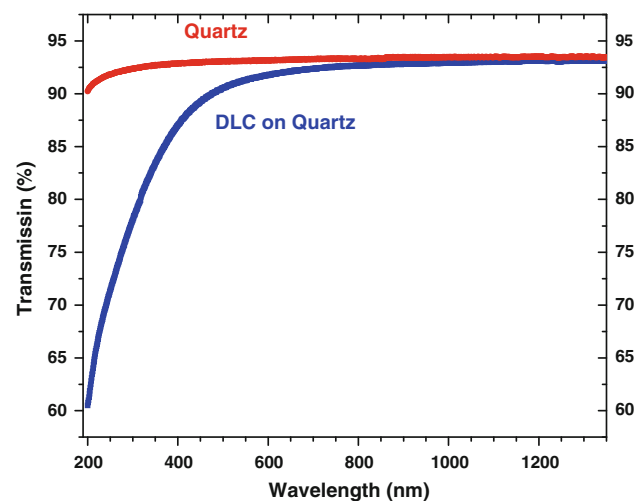
Fig. 6 Spectrophotometer transmission spectrum for 25 nm DLC grown on quartz, with quartz reference

3.2 Damage threshold

Released DLC films on metal plate holders were placed at the focus of the 1,064 nm wavelength laser. The laser energy was varied primarily through a combination of neutral density filters, although the laser controller could adjust the energy in nonlinear steps. The power of the laser at the typical controller setting was measured to be, on average, 24 mW at 10 Hz repetition rate or 2.4 mJ per shot. The fluence at 90, 70, and 50 % energy contours was 61, 81, and 95 J/cm^2. The maximum output of the laser was 209 J/cm^2 at 90 % energy contour, at this focus. Various combinations of neutral density filters were used to reduce the laser energy and have finer control over laser fluence increments.

The threshold was found by reducing the laser fluence using many neutral density filters and then reducing the filters in minimal steps. The film was then inspected under a microscope to find the level of damage delivered. Therefore, each shot of the laser occurred with relatively large time gaps (on the order of minutes) compared to the irradiation time (6 ns). Since the current purpose for the film for ion generation and its requirements is that it can survive the laser prepulse, minor damage is acceptable. This is because the topography of the film is expected to deform at the acoustic speed, which is slow enough that the ultrahigh-intensity laser pulse will arrive first.

For the film shot in Fig. 7, the initial shots do minor damage to the film since it is well below the damage threshold of the film. From the coefficient of extinction measured and shown in Fig. 5, the DLC film has very little absorption in the near infrared. Therefore, the damage is likely due to graphite debris from the target during deposition.

During multiple shots, the films at the damage locations are expected to absorb more NIR laser light due to the graphitization of the film with each successive shot; thus, the damage threshold (when the film finally breaks) is expected to be lower than for a single shot threshold. When the damage site is viewed at 200× magnification, the film

is seen to still be continuous, although it has been deformed to bulge away from the incident laser.

For a single shot, the damage threshold was 17 J/cm^2 at 90 % energy contour for a film with a typical amount of debris. Figure 8 shows the confocal images of such a DLC film, showing the depth profile of the crater formed on the freestanding film when subjected to a single pulse at 15 J/cm^2 laser fluence at 90 % energy contour. The highest damage threshold for a smooth film was found to have a peak fluence of 405 J/cm^2 or peak intensity of 7×10^{10} W/cm^2. The corresponding fluencies at 90, 50, 30, and 10 % energy contours are 189, 292, 336, and 376 J/cm^2, respectively. This occurred after 13 laser pulses with no apparent damage dealt by the initial pulses until the film was destroyed by the final pulse. We expect this is a sign of a film highly free of debris from PLD. Similar multishot studies were carried out on commercial Si_3N_4 (Norcada 500 μm × 500 μm × 0.1 μm freestanding film) which displayed a much more consistent threshold at 138 J/cm^2 at 90 % energy contour or 314 J/cm^2 peak fluence.

Optical breakdown and material damage in a transparent optical material by ns laser pulses are due to photoionization and avalanche ionization [17, 18]; however, defects and inclusions on the surface and inside of the optical material can initiate localized breakdown and lead to the significant lowering of the damage threshold fluences [19–21]. In general, the damage threshold is high for a high-quality, clean, and low-defect optical material. For example, for high-quality low-defect fused silica, under the irradiation of 1 ns and 1 μm laser pulses, a damage threshold fluence of approximately 40 J/cm^2 was observed [17]. It was also observed a $\tau^{1/2}$ dependence of the threshold damage fluence upon pulse duration τ [17].

The damage threshold peak fluence of 314 J/cm^2 for freestanding film of Si_3N_4 is surprising. The fluence is an order of magnitude higher than typical damage threshold fluences for bulk optical materials including fused silica and many glasses [22]. The reason the 100-nm-thick freestanding optical film has a significantly higher damage threshold is likely due to a much smaller interaction
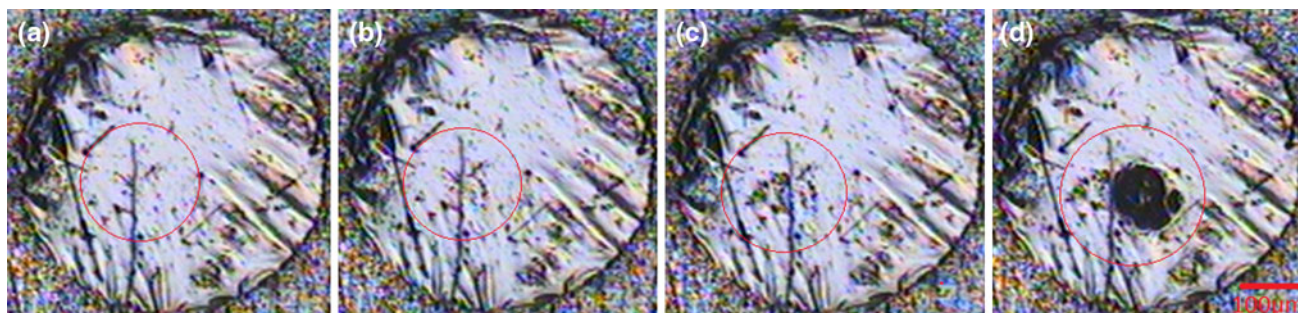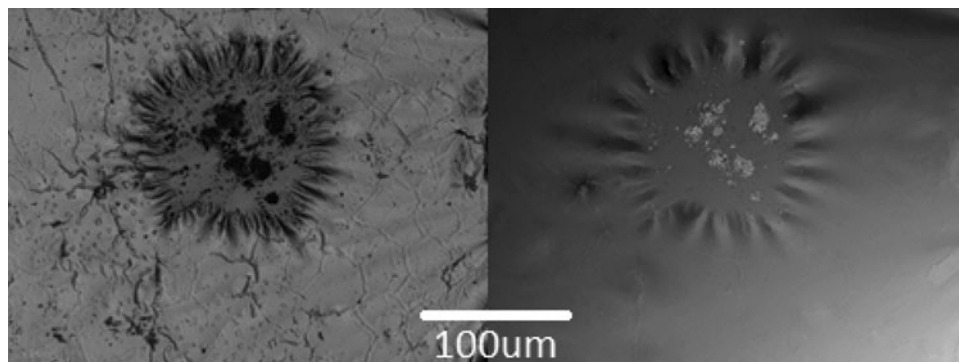

Fig. 7 40× Magnification: 100-nm-thick DLC film 500 μm in diameter shot on the indicated location multiple times with increasing laser fluence **a** 3.1 J/cm^2 **b** 4.9 J/cm^2 **c** 6.1 J/cm^2 **d** 7.7 J/cm^2 at 90 % energy contour

Fig. 8 Confocal images of the crater formed on the freestanding DLC film when subjected to 15 J/cm² laser fluence

volume of material irradiated by the laser beam. This leads to the reduction in the probability of encountering a defect or inclusion. To give confidence that the above values are deduced correctly, the same setup was used to determine damage threshold fluences for several additional materials. Table 1 gives the damage threshold peak fluences for the previous two freestanding foils and the additional materials. Our laser damage threshold fluence values are consistent with the reported values for copper and graphite, when they are scaled for laser pulses with $\tau = 6$ ns assuming a $\tau^{1/2}$ dependence. These values are compared to 90 % energy contour values since sources use either $1/e^2$ [23, 24] or an unspecified average [25–27] fluence calculation. "Damage threshold" was defined in our work by visible damage of the film when viewed under optical microscope (up to 200× magnification). Other methods exist: measuring [25] or estimating [27] ablated material mass and extrapolating to "no mass lost" or 50 % probability of visible damage [24].

The laser damage thresholds for freestanding diamond-like carbon films are not available but there are several reports for those of bulk diamond. The damage threshold intensity for type-IIa single crystal diamond film (0.94 mm) was reported to be 3.0×10^{12} W/cm² when it

was irradiated with 30 ps, 1,064 nm laser pulses giving a damage threshold fluence of 90 J/cm² [28]. Another damage threshold intensity value for type-IIa bulk diamond (two 8 mm² unfinished faces and one 2.5 mm² polished face available) was reported to be 1.6×10^{11} W/cm² when it was irradiated with 30 ns, 1 μm laser pulses giving a damage threshold fluence of 4,800 J/cm² [29]. The two values are consistent with each other if the threshold damage fluence follows a $\tau^{1/2}$ dependence. Other damage threshold values reported [30–32] for single crystal or polycrystalline diamonds with 1 μm laser irradiation were significantly lower than the above two values (0.8–21.5 J/cm², scaled to 6 ns pulse). One explanation for the significantly lower damage threshold values is the presence of graphitic inclusions [31]. The damage threshold fluence reported in [29] for bulk diamond would be approximately 2,000 J/cm² when scaled to a 6 ns, 1 μm laser pulse. The value is several times higher than the maximum laser damage threshold fluence of our 100 nm freestanding DLC film. This is a reasonable result because the absorption edge of diamond is at a shorter wavelength than the DLC, and thus, diamond requires higher laser intensity for multiphoton absorption. The laser damage thresholds for our freestanding DLC film, similar to those of diamond films, vary significantly from sample to sample probably because of graphitic inclusions introduced by target debris during the PLD deposition process [33].

The number of debris in PLD-produced DLC thin film can be significant as pointed out by our previous studies [33]. We reported a count of 25,000 debris/cm²/nm with size >100 nm on a 30-nm-thick DLC thin film produced by PLD at a higher laser intensity of 6 GW/cm². Graphite has a relatively high coefficient of extinction ($k = 2.02$, $\lambda = 1$ μm) [34] compared to diamond ($k \approx 0$, $\lambda = 1$ μm) [34] and our film ($k \approx 0$, $\lambda = 1$ μm) in Fig. 5. Therefore, at one compositional extreme, graphite (100 % sp^2) absorbs more laser energy and has a lower threshold than diamond (100 % sp^3) at the other extreme. The high absorption of photons in graphite can produce seed electrons, which lead to avalanche ionization [17] on the film.

Table 1 Damage thresholds compared with reported materials

Samples	Laser damage threshold fluence (J/cm²)		
	(This work)		(Other reported data scaled to 6 ns)
	Peak fluence	90 % Energy contour	
100 nm Freestanding DLC	405 (max.)	189 (max.)	No data found
100 nm Freestanding Si₃N₄	315	138	No data found
100 nm Si₃N₄ on Si	18	16	13.8 [23]
Bulk Copper	13	6	10.7 [24]; 6.7 [25]
200 μm Graphite foil	4	2	1.1 [26]; 1.1 [27]

The graphite debris can also cause damage to the film due to heating, and thus, films with little or no graphite debris will demonstrate a high damage threshold. There are a number of methods which can be used to eliminate debris: using a liquid target [35], mechanical shuttering [36], and magnetic guidance of the laser-produced plasma [33, 37, 38]. Previous work has been performed to reduce graphite debris using magnetically guided pulsed laser deposition (MGPLD) [33, 37, 38]. For the MGPLD growths [38], a 1-kG magnetic field generated by a curved solenoid was used to guide carbon plasma while allowing debris particles to expand freely. Twenty times debris reduction was reported with this method for DLC films [33] and it was also observed that DLC films produced by MGPLD had better diamond-like characteristics compared to DLC films grown using conventional PLD [38].

The current wisdom [1–7] suggests that the ultrahigh-intensity laser pulses used for irradiating the ultrathin DLC foils must have extremely low prepulse level. This is in order to avoid damaging the DLC foil before the arrival of the main ultrashort laser pulse. All the experiments so far were conducted using specialized, extremely high-contrast laser system such as the Trident system in Los Alamos National Laboratory [2] or employing double plasma mirror [3] to significantly reducing the prepulse level. The ultrahigh-contrast lasers have a typical prepulse to main pulse intensity contrast ratio of $\sim 10^{-10}$–10^{-12} [39, 40], whereas a typical system has a ratio of $\sim 10^{-7}$ [9, 40]. High-energy ions discussed earlier were produced with a peak laser intensity of 7×10^{19} W/cm^2 [2]. In this study, we found that for our best freestanding ultrathin DLC foil, its damage threshold can have a peak intensity as high as 7×10^{10} W/cm^2. Therefore, we would require a contrast ratio of 10^{-10}. By optimizing the Pockels cell timing, reduction in the prepulse energy by an order of magnitude has been achieved and results in a required contrast ratio of $\sim 10^{-9}$. With film optimization, it may be possible to further improve the damage threshold of the film through the reduction in debris as discussed above. These films have an sp^3 content of 23 % and already have an very small coefficient of extinction at 1 μm wavelength. Therefore, it may not be necessary to have films with extremely high sp^3 content when working in near-infrared regime. The lift-off and transfer technique could be optimized for DLC to eliminate wrinkles, such as those seen near the edged in Fig. 7, which would enable better quality targets and give more repeatable results. If typical laser systems with good contrast can be used without resorting to specialized laser systems with extremely high contrast, this could significantly increase the number of available laser systems for experiments using ultrathin freestanding DLC foils in ion-driven fast ignition and laser-driven ion therapy research since laser systems with good contrast far outnumber laser systems with extremely high contrast.

4 Conclusions

Freestanding DLC films were fabricated using PLD deposition on soap-covered substrate. They were characterized using AFM to have 0.6 nm rms surface roughness for DLC deposited on silicon and 9 nm for freestanding films which agrees with that of the soap film. XPS revealed 23 % sp^3, 73 % sp^2, and 3 % C–O bonding proportions. Film hardness was determined to be 10 GPa on a 100 nm DLC film for force loading of 100–4,500 μN. Damage threshold measurements were taken using 1,064 nm wavelength of Nd:YAG nanosecond pulsed laser. A maximum damage threshold with a peak intensity of 7×10^{10} W/cm^2 was found for our best ultrathin freestanding DLC foil. The results suggest that with film optimization, typical laser systems with good contrast may be possible candidates for experiments utilizing ultrahigh intensity to produce high-energy ions. This could significantly increase the number of available laser systems for experiments in ion-driven fast ignition and laser-driven ion therapy research using such targets.

References

1. VKh Liechtenstein, T.M. Ivkova, E.D. Olshanski, R. Repnow, J. Levin, R. Hellborg, P. Persson, T. Schenkel, Nucl. Instrum. Meth. Physic. Res. A **480**, 185 (2002)
2. L. Yin, B.J. Albright, B.M. Hegelich, J.C. Fernandez, Laser Part. Beams **24**, 291 (2006)
3. A. Henig, D. Kiefer, K. Markey, D.C. Gautier, K.A. Flippo, S. Letzring, R.P. Johnson, T. Shimada, L. Yin, B.J. Albright, K.J. Bowers, J.C. Fernandez, S.G. Rykovanov, H.C. Wu, M. Zepf, D. Jung, V.K. Liechtenstein, J. Schreiber, D. Habs, B.M. Hegelich, Phys. Rev. Lett. **103**, 045002 (2009)
4. A.P.L. Robinson, M. Zepf, S. Kar, R.G. Evans, C. Bellei, New J. Phys. **10**, 013021 (2008)
5. L. Yin, B.J. Albright, D. Jung, K.J. Bowers, R.C. Shah, S. Palaniyappan, J.C. Fernandez, B.M. Hegelich, Phys. Plasmas **8**, 053103 (2011)
6. A. Henig, S. Steinke, M. Schnurer, T. Sokollik, R. Horlein, D. Kiefer, D. Jung, J. Schreiber, B.M. Hegelich, X.Q. Yan, J. Meyer-ter-Vehn, T. Tajima, P.V. Nickles, W. Sandner, D. Habs, Phys. Rev. Lett. **103**, 245003 (2009)

7. D. Jung, L. Yin, B.J. Albright, D.C. Gautier, R. Horlein, D. Kiefer, A. Henig, R. Johnson, S. Letzring, S. Palaniyappan, R. Shah, T. Shimada, X.Q. Yan, K.J. Bowers, T. Tajima, C. Fernandez, D. Habs, B.M. Hegelich, Phys. Rev. Lett. **107**, 115002 (2011)

8. J.C. Fernandez, J.J. Honrubia, B.J. Albright, K.A. Flippo, D.C. Gautier, B.M. Hegelich, M.J. Schmitt, M. Temporal, L. Yin, Nucl. Fusion **49**, 065004 (2009)

9. S. Auer, V. Hable, C. Greubel, G.A. Drexler, T.E. Schmid, C. Belka, G. Dollinger, A.A. Friedl, Radiat. Oncol. **6**, 139 (2011)

10. S. Le Pape, Y.Y. Tsui, A. Macphee, D. Hey, P. Patel, A. Mackinnon, M. Key, M. Wei, T. Ma, F.N. Beg, R. Stephens, K. Akli, T. Link, L. Van-Woerkom, R.R. Freeman, Opt. Lett. **34**, 1997 (2009)

11. M. Gupta, F.R. Chowdhury, V. Sauer, Y.Y. Tsui, Proc. SPIE **8007**, 80070J (2011)

12. F.C. Tai, S.C. Lee, C.H. Wei, S.L. Tyan, Mater. Transact. **47**(7), 1847 (2006)

13. H. Minami, D. Manage, Y.Y. Tsui, R. Fedosejevs, M. Malac, R. Egerton, Appl. Phys. A **73**, 531 (2001)

14. R. Delmdahl, S. Weissmantel, G. Reisse. Adv. Mater. Process **23** (2010)

15. S.B. Singh, M. Pandey, N. Chand, A. Biswas, D. Bhattacharya, S. Dash, A.K. Tyagi, R.M. Dey, S.K. Kulkarni, D.S. Patil, Bull. Mater **31**, 5813 (2008)

16. B. Mednikarov, G. Spasov, Tz Babeva, J. Pirov, M. Sahatchieva, C. Popov, W. Kulisch, J. Optoelectron. Adv. Mater **7**, 3 1407 (2005)

17. B.C. Stuart, M.D. Feit, S. Herman, A.M. Rubenchik, B.W. Shore, M.D. Perry, Phys. Rev. B **54**, 1749 (1996)

18. C.B. Schaffer, A. Brodeur, E. Mazur, Meas. Sci. Technol. **12**, 1784 (2001)

19. R.A. Negres, M.D. Feit, S.G. Demos, Opt. Express **18**, 10642 (2012)

20. C.W. Carr, H.B. Radousky, A.M. Rubenchik, M.D. Feit, S.G. Demos, Phys. Rev. Lett. **92**, 087401 (2004)

21. M.D. Feit, A.M. Rubenchik, D.R. Faux, R.A. Riddle, A.B. Shapiro, D.C. Eder, B.M. Penetrante, D. Milam, F.Y. Genin, M.R. Kozlowski, Proc. SPIE **2966**, 417 (1997)

22. J.H. Campbell, F. Rainer, M.R. Kozlowski, C. Robert Wolfe, I.M. Thomas, F.P. Milanovich, Proc. SPIE **1441**, 444 (1990)

23. A. Schoonderbeek, V. Schutz, O. Haupt, U. Stute, J. Laser Micro/Nanoengineer. **5**, 248 (2010)

24. Y. Jee, M.F. Becker, R.M. Walser, J. Opt. Soc. Am. B **5**, 648 (1988)

25. L. Torrisi, S. Gammino, L. Ando, V. Nassisi, D. Doria, A. Pedone, Appl. Surface Sci. **210**, 262 (2003)

26. A. Semerok, S.V. Fomichev, F. Brygo, P.-Y. Thro, C. Grisolia, J. Nucl. Mater. **420**, 198 (2012)

27. F. Le Guern, C. Hubert, S. Mousset, E. Gauthier, C. Blanc, P. Wodling, J.M. Weulersse, J. Nucl. Mater. **335**, 410 (2004)

28. P. Liu, R. Yen, N. Bloembergen, IEEE J. Quant. Electron. **14**, 574 (1978)

29. A.M. Kondyrev, Y.V. Tarasova, A.E. Chmel, Sov. J. Opt. Technol. **59**, 654 (1992)

30. C.A. Klein, R. DeSalvo, Appl. Phys. Lett. **63**, 1895 (1993)

31. S. Albin, L. Watkins, K. Ravi, S. Yokota, Appl. Phys. Lett. **54**, 2728 (1989)

32. R.S. Sussmann, G.A. Scarsbrook, C.J.H. Wort, Diam. Relat. Mater. **3**, 1173 (1994)

33. Y.Y. Tsui, H. Minami, D. Vick, R. Fedosejevs, J. Vac. Sci. Technol. A **20**, 744 (2002)

34. E.D. Palik, *Handbook of Optical Constants of Solids* (Elsevier London, UK, 1998)

35. M. Hanabusa, K. Tsujihara, J. Appl. Phys. **78**, 4267 (1995)

36. D. Lubben, S.A. Barnett, K. Suzuki, S. Gorbatkin, J.E. Greene, J. Vac. Sci. Technol. B **3**, 968 (1985)

37. Y.Y. Tsui, D. Vick, R. Fedosejevs, Appl. Phys. Lett. **70**, 1953 (1997)

38. H. Minami, *M* (University of Alberta, Edmonton, Alberta, Canada, Sc. Thesis, 1999)

39. J.C. Shah, R.P. Johnson, T. Shimada, K.A. Flippo, J.C. Fernandez, B.M. Hegeligh, Opt. Lett. **34**, 15 2273 (2009)

40. S. Steinke, A. Henig, M. Schnürer, T. Sokollika, P.V. Nickles, D. Jung, D. Kiefe, R. Hörlein, J. Schreiber, T. Tajima, X.Q. Yan, M. Hegelich, J. Meyer-ter-Vehn, W. Sandner, D. Habs, Laser Part. Beams **28**, 215 (2010)